A Prokaryotic Membrane Sculpting BAR Domain Protein

Daniel A. Phillips[1*], Lori A. Zacharoff[2*], Cheri M. Hampton[3], Grace W. Chong[4], Anthony P. Malanoski[5], Lauren Ann Metskas[6], Shuai Xu[2], Lina J. Bird[5], Brian J. Eddie[5], Grant J. Jensen[6,7], Lawrence F. Drummy[3], Mohamed Y. El-Naggar[2,4,8], and Sarah M. Glaven[5]

[1]American Society for Engineering Education, Washington, DC, USA.
[2]University of Southern California, Department of Physics and Astronomy, Los Angeles, CA 90089
[3]Materials and Manufacturing Directorate, Air Force Research Laboratory, Wright-Patterson Air Force Base, WPAFB, OH, USA.
[4]University of Southern California, Department of Biological Sciences, Los Angeles, CA 90089
[5]Center for Bio/Molecular Science and Engineering, Naval Research Laboratory, Washington, DC, USA.
[6]California Institute of Technology, Division of Biology and Biological Engineering, Pasadena, CA 91125
[7]California Institute of Technology, Howard Hughes Medical Institute, Pasadena, CA 91125
[8]University of Southern California, Department of Chemistry, Los Angeles, CA 90089

[*]These authors contributed equally to this work

Send all correspondence to:
Daniel A. Phillips
Daniel.phillips.ctr@nrl.navy.mil
4555 Overlook Ave.
Washington, DC 20375

Lori Zacharoff
zacharof@usc.edu
920 Bloom Walk
SSC, 215C
Los Angeles, CA 90089

Summary Paragraph

Bin/Amphiphysin/RVS (BAR) domain proteins belong to a ubiquitous superfamily of coiled-coil proteins that influence membrane curvature in eukaryotes and are associated with vesicle biogenesis, vesicle-mediated protein trafficking, and intracellular signaling[1-6]. BAR domain proteins have not been identified in bacteria, despite certain organisms displaying an array of membrane curvature phenotypes[7-16]. Here we identify a prokaryotic BAR domain protein, BdpA, from *Shewanella oneidensis* MR-1, an iron reducing bacterium known to produce redox active membrane vesicles and micrometer-scale membrane extensions. BdpA is required for uniform size distribution of outer membrane vesicles and is responsible for scaffolding outer membrane extensions (OMEs) into membrane structures with consistent diameter and curvature. While a strain lacking BdpA produces OMEs, cryogenic transmission electron microscopy reveals more lobed, disordered OMEs rather than the membrane tubes produced by the wild type strain. Overexpression of BdpA promotes OME formation even during planktonic conditions where *S. oneidensis* OMEs are less common. Heterologous expression also results in OME production in *Marinobacter atlanticus* CP1 and *Escherichia coli*. Based on the ability of BdpA to alter membrane curvature *in vivo*, we propose that BdpA and its homologs comprise a newly identified class of prokaryotic BAR (P-BAR) domains that will aid in identification of putative P-BAR proteins in other bacterial species.

Introduction

Eukaryotic Bin/Amphiphysin/Rvs (BAR) domain-containing proteins generate membrane curvature through electrostatic interactions between positively charged amino acids and negatively charged lipids, scaffolding the membrane along the intrinsically

curved surface of the antiparallel coiled-coil protein dimers[17-20]. Some BAR domain-containing proteins, such as the N-BAR protein BIN1, contain amphipathic helical wedges that insert into the outer membrane leaflet and can assist in membrane binding[21]. Other BAR domains can be accompanied by a membrane targeting domain, such as PX for phosphoinositide binding[22,23], in order to direct membrane curvature formation at specific sites, as is the case with sorting nexin BAR proteins[4]. The extent of accumulation of BAR domain proteins at a specific site can influence the degree of the resultant membrane curvature[24], and tubulation events arise as a consequence of BAR domain multimerization in conjunction with lipid binding[25]. Interactions between BAR domain proteins and membranes resolve membrane tension, promote membrane stability, and aid in localizing cellular processes, such as actin binding, signaling through small GTPases, membrane vesicle scission, and vesicular transport of proteins[1,26,27]. Despite our knowledge of numerous eukaryotic BAR proteins spanning a variety of modes of curvature formation, membrane localizations, and subtypes (N-BAR, F-BAR, and I-BAR), characterization of a functional prokaryotic BAR domain protein has yet to be reported.

Bacterial cell membrane curvature can be observed during the formation of outer membrane vesicles (OMV) and outer membrane extensions (OME). OMV formation is ubiquitous and has many documented functions[9]. OMEs are less commonly observed, remain attached to the cell, and various morphologies can be seen extending from single cells including *Myxococcus xanthus*[14,15], flavobacterium strain Hel3_A1_48[8], *Vibrio vulnificus*[10], *Francisella novicida*[28], *Shewanella oneidensis*[7,29-31], and as cell-cell connections in *Bacillus subtilis*[32-34] and *Eschericia coli*[35]. Several bacterial proteins have demonstrated membrane tubule formation capabilities *in vitro*[16,36-40], but despite the

47 growing number of reports, proteins involved in shaping bacterial membranes into
48 OMV/Es have yet to be identified. Recently, researchers have begun to suspect that OMV
49 and OME formation has some pathway overlap[8], and it is proposed that proteins are
50 necessary to stabilize these structures[13].

51 *Shewanella oneidensis* is a model organism for extracellular electron transfer
52 (EET), a mode of respiration whereby electrons traverse the inner membrane, periplasm,
53 and outer membrane via multiheme cytochromes to reach exogenous insoluble terminal
54 electron acceptors, such as metals and electrodes[41,42]. It is also known to produce redox-
55 active OMVs[43] and OMEs coated with mulitheme cytochromes, particularly upon surface
56 attachment[7,30,43]. However, little is known about their formation mechanism, control of
57 shape or curvature, and electrochemical properties that influence EET function.

58 **Results and Discussion**

59 ***S. oneidensis* OMVs are redox-active and enriched with BdpA**

60 OMVs were purified from cells grown in batch cultures to characterize the redox
61 features and unique proteome of *S. oneidensis* OMVs, as well as to identify putative
62 membrane shaping proteins. Cryogenic transmission electron microscopy (cryo-TEM)
63 tomography reconstruction slices of the purified samples showed uniform OMVs with the
64 characteristic single membrane phenotype and an approximate diameter of 200 nm (Fig.
65 1a). Previous measurements suggest OMVs can reduce extracellular electron
66 acceptors[43] and that vesicles from *G. sulfurreducens* can mediate electron transfer[44].
67 Electrochemical activity of multiheme cytochrome complex MtrCAB and their ability to
68 mediate micrometer-scale electron transport has been characterized in whole cells[45], but
69 no electrochemical characterization of OME/Vs has been reported that link activity to

multiheme cytochromes. Here, electrochemical measurements of isolated OMVs were performed to determine if purified OMVs maintain the redox features when detached from cells. Cyclic voltammetry (CV) of isolated membrane vesicles adhered to a gold electrode via self-assembled monolayers show redox activity demonstrating electron transfer to and from the electrode interface (Fig. 1b). The first derivative (Fig. 1b inset) revealed a prominent peak with a midpoint potential of 66 mV and a smaller peak at -25 mV versus a standard hydrogen reference electrode (SHE). This midpoint potential is consistent with the characteristics of multiheme cytochromes such as MtrC/OmcA from previous microbial electrochemical studies[45,46], suggesting that the extracellular redox molecules of the cellular outer membrane extends to OMVs.

The proteome of the OMVs was compared to the proteome of purified outer membranes extracted from whole cells. Using a label-free quantification method[47], significant differences in the ratio of individual proteins in the vesicle to the outer membrane could be computed (log fold change) (Fig 1c). The proteome of the purified OMVs showed ~300 proteins were significantly enriched in the vesicles as compared to the outer membrane, and ~300 proteins were significantly excluded from the vesicles (Fig. 1c). MtrCAB cytochromes were neither significantly enriched nor excluded from the vesicles, consistent with the interpretation that vesicles could extend the respiratory surface area. Active protein sorting into eukaryotic vesicles is a coordinated process involving a protein sorting signal, localized membrane protein recruitment, initiation of membrane curvature induction, and coating nascent vesicles with membrane scaffolds[48]. Several proteins significantly enriched in the vesicles might contribute to OMV formation, such as murein transglycosylase, the peptidoglycan degradation enzyme holin, cell

93 division coordinator CpoB, and a highly enriched putative BAR domain-containing protein
94 encoded by the gene at open reading frame SO_1507, hereafter named BAR domain-
95 like protein A (BdpA) (Fig. 1d).

96 Vesicle enrichment of BdpA led us to the hypothesis that BdpA could be involved
97 in membrane shaping of OMVs based on the role of such proteins in eukaryotes. The C-
98 terminal BAR domain of BdpA is predicted to span an alpha-helical region from AA 276-
99 451 (E-value = 2.96e-03); however, since the identification of the protein is based on
100 homology to the eukaryotic BAR domain consensus sequence (cd07307), it is possible
101 that the BAR domain region extends beyond these bounds (Fig. 1d). Coiled coil
102 prediction[49] suggests BdpA exists in an oligomeric state of antiparallel alpha-helical
103 dimers, as is the case for all known BAR domain proteins[18,50-52]. BdpA has an N-terminal
104 signal peptide with predicted cleavage sites between amino acids 22-23, suggesting non-
105 cytoplasmic localization (Fig. 1d). A galactose-binding domain-like region positioned
106 immediately downstream of the signal peptide supports lipid targeting activity seen in
107 other BAR domain proteins, such as the eukaryotic sorting nexins[3] which have phox (PX)
108 domains that bind phosphoinositides[53]. The *S. oneidensis* rough-type lipopolysaccharide
109 (LPS) contains 2-acetamido-2-deoxy-D-galactose[54], which suggests possible localization
110 of the protein to the outer leaflet of the outer membrane.

111 **BdpA controls size distribution of vesicles**

112 To determine whether BdpA influences vesicle morphology, OMVs were harvested
113 from wild type (WT) cells and cells in which the gene for BdpA had been deleted (Δ*bdpA*),
114 and their diameters were measured by dynamic light scattering (DLS). WT OMVs (n=11)
115 had a median diameter of 190 nm with little variability in the population (±21 nm), while

the diameters of Δ*bdpA* OMVs (n=9) were distributed over a wider range with a median value of 280 nm ± 131 nm (Fig 2a). The data suggest BdpA controls vesicle diameter in membrane structures *ex vivo*, potentially acting by stabilizing OMVs. OMV frequency and size distribution was also measured in live cultures using a perfusion flow imaging platform and the membrane stain FM 4-64, as described previously[29]. *S. oneidensis* strains were monitored for OME/V production over the course of 5 hours (>5 fields of view per replicate, n=3). Spherical membrane stained extracellular structures were classified as OMVs, while larger aspect ratio (i.e. length greater than the width) structures were classified as OMEs. The duration of time-lapse imaging allowed tracking the progression of an OME/V over time. It was possible to quantify the proportion of cells producing 'large' vesicles, defined as those where the membrane was clearly delineated from the interior of the vesicles, typically >300 nm. Δ*bdpA* cells produced significantly more large vesicles compared to WT cells (Fig. 2b) even though both the overall frequency of vesiculation and extensions were the same (Fig. 2c). The size of *S. oneidensis* vesicles was more discrete than vesicles produced by other bacteria[55,56] that do not contain a BdpA homolog, making it likely that BdpA is responsible for precise regulation of vesicle size. Previous studies showed that OMEs transition between large vesicles and OMEs over time[29]. BdpA appears to be involved in this transition due to the increased frequency of large vesicles from Δ*bdpA* cells.

BdpA constrains membrane extension morphology

The median diameter of the OMVs is also the apparent maximum diameter observed in outer membrane extensions[29] suggesting BdpA influences membrane morphologies of both structures. As with the vesicles, WT and Δ*bdpA* cells made the

same number of extensions in perfusion flow conditions (Fig. 2c). The resolution of fluorescence microscopy was insufficient to identify morphological differences between OMEs. To minimize sample processing of unfixed OMEs for cryo-TEM sample preparation, cells were deposited onto a glass coverslip instead of a perfusion flow chamber. BdpA was also expressed from a 2,4-diacetylphloroglucinol (DAPG)-inducible promoter[57] (P_{PhlF}-BdpA) in the Δ*bdpA* strain containing the plasmid p452-*bdpA*. After 3 hours post deposition on cover glass, OMEs can be seen extending from WT, Δ*bdpA*, and Δ*bdpA* p452-*bdpA* cells (Fig. 3, Supplemental Fig. 1, 5 fields of view, n=3). Similar to perfusion flow experiments (Fig. 2c), no statistically significant difference in the overall frequency of OME production was observed between the cells in static cultures.

Cryo-TEM was used to assess any morphological differences between the OMEs in each of the strains at the ultrastructural level. *S. oneidensis* OMEs from unfixed WT, Δ*bdpA,* and Δ*bdpA* p452-*bdpA* strains were visualized at 90 minutes (Supplemental Fig. 2) and 3 hours (Fig. 3) post deposition onto EM grids. At 90 minutes, WT OME phenotypes appeared narrow, tubule-like, and seldom interspersed with lobed regions (Supplemental figure 2a). In Δ*bdpA* OMEs, lobed regions are prevalent with irregular curvature (Supplemental figure 2b). Several narrow Δ*bdpA* p452-*bdpA* OMEs evenly interspersed with slight constriction points or "junction densities" were observed extending from a single cell (Supplemental Fig. 2c), suggesting that BdpA expression rescues the phenotype by constricting and ordering OMEs into narrow tubules. By 3 hours post inoculation, images of WT cells consistently show narrow, tubule-like OMEs (Fig. 3b, n=31). The Δ*bdpA* OMEs generally appear as lobed, disordered vesicle chains with irregular curvature, and vesicles can be observed branching laterally from lobes on the

extensions (Fig. 3b, n=13). Nascent WT OMEs from previous studies also exhibited lateral branching of vesicles and lobes, but they exhibited uniform curvature and diameter between lobes and were observed immediately following OME formation[29]. Tubules were not observed in any Δ*bdpA* OMEs at 3 hours. OMEs from Δ*bdpA* p452-*bdpA* cells appear as a narrow tubules of a uniform curvature or as ordered vesicle chains (Fig. 3b, n=3).

Expression of BdpA results in OMEs during planktonic growth

S. oneidensis OMEs are more commonly observed during surface attachment rather than planktonic cultures[7,29]. BAR domain proteins can directly promote tubule formation from liposomes *in vitro*[24], so inducing expression of an additional copy of the *bdpA* gene prior to attachment could result in OME formation even during planktonic growth. Growth curves were similar in cultures with the pBBR1-mcs2 empty vector in either of the WT (MR-1 pBBR1-mcs2) or Δ*bdpA* (Δ*bdpA* pBBR1-mcs2) background strains, but induction of *bdpA* in Δ*bdpA* p452-*bdpA* cells at higher concentrations of 1.25 and 12.5 μM 2,4-diacetylphloroglucinol affected the growth rate (Supplemental figure 3). Planktonic cultures inoculated from overnight cultures were induced with 12.5 μM DAPG for 1 hour, labeled with FM 4-64, and imaged by confocal microscopy. Neither WT (Fig. 4) nor MR-1 pBBR1-mcs2 exposed to 12.5 μM DAPG (not shown) produced OMEs immediately following deposition onto cover glass. However, 12.5 μM DAPG-induced *S. oneidensis* MR-1 p452-*bdpA* cells displayed OMEs immediately, ranging between 1-7 extensions per cell (Figure 4, Supplemental video 1). OME formation combined with growth rate data suggests *bdpA* expression in planktonic cultures redirects membrane production necessary for cell division into OMEs. The ultrastructure of OMEs resulting from expression of *bpdA* from MR-1 p452-*bdpA* cells was examined by cryo-TEM, but in

this case samples from planktonic cultures were vitrified on EM grids after induction rather than incubation during induction on the EM grids. OMEs appear as tubule-like segments interspersed with pearled regions proximal to the main cell body (Fig. 4b). OMEs from the MR-1 p452-*bdpA* strain are observed as thin, tubule-like outer membrane vesicle chains, suggesting BdpA involvement in the constriction of the larger outer membrane vesicle chains into longer, tubule-like extensions with more evenly interspersed junction densities. The BdpA OME phenotype more closely resembles membrane tubules formed by the F-BAR protein Pacsin1 from eukaryotic cells, showing a mixture of tubule regions interspersed with pearled segments[58,59].

BdpA-mediated membrane extensions in *Marinobacter atlanticus* CP1 and *E. coli*.

To test the effect of expressing BdpA in an organism with no predicted BAR domain-containing proteins and no apparent OME production, BdpA was expressed in *Marinobacter atlanticus* CP1[60]. *Marinobacter* and *Shewanella* are of the same phylogenetic order (Alteromonadales) and have been used for heterologous expression of other *S. oneidensis* proteins, such as MtrCAB[61,62]. Upon exposure to DAPG, *M. atlanticus* containing the p452-*bdpA* construct (CP1 p452-*bdpA*) form membrane extensions (Figure 4). OMEs ranged from small membrane blebs to OME tubules extending up to greater than 10 μm in length from the surface of the cell (Supplemental Fig. 4). As noted previously, variation in the tubule phenotypes are commonly seen in tubules from eukaryotic F-BAR proteins[58,59], showing possible mechanistic overlap of mutable membrane curvature functionalities between these two separate BAR domain proteins.

In previous membrane curvature formation experiments with eukaryotic BAR domain proteins, localized BAR domain protein concentrations affected the resultant shape of the membranes, ranging from bulges to tubules and branched, reticular tubule networks at the highest protein densities[63-65]. We predicted that expression of BdpA in cells optimized for protein overexpression, such *E. coli* BL21(DE3), would show OMEs resembling structures previously observed from eukaryotic BAR protein experiments *in vitro*. While the uninduced *E. coli* BL21(DE3) p452-*bdpA* cells had uniform, continuous cell membranes similar to those of plasmid-free BL21(DE3) cells under the conditions tested, *E. coli* BL21(DE3) cells containing the p452-*bdpA* vector induced with DAPG had outer membrane extensions and vesicles (Figure 4). When visualized over time, OMEs progressed towards a network of reticular membrane structures extending from the cell (Fig. 4c). After 30 minutes, additional membrane blebs were observed that developed into elongated OMEs by 60 minutes. Growth of *E. coli* OMEs was coincident with shrinking of the cell body (from initial cell length = 4.457 μm to 3.479 μm at 60 minutes), supporting direct membrane sculpting activity of BdpA.

P-BAR: a new BAR domain subtype

The discovery of a novel, functional BAR domain protein in prokaryotes provokes questions into the evolutionary origin of BAR domains, such as whether the BdpA BAR domain in *Shewanella* arose as a result of convergent evolution, a horizontal gene transfer event, or has a last common ancestor across all domains of life. BdpA homologs were identified by PSI-BLAST in several other organisms, ranging from other species of *Shewanella* to *Alishewanella*, *Rheinheimera*, and *Cellvibrio* (Supplemental Fig. 5). The current BAR domain pfam Hidden Markov Model (HMM) prediction analysis identified

BAR domain features in only 5 of the 52 prokaryotic homologs despite greater than 90% homology to *S. oneidensis* BdpA. Functional analysis will be necessary to determine if these homologs contain unpredicted BAR domains and merit inclusion in the generation of a new BAR domain pfam seed alignment. The resultant alignment was used to generate a maximum likelihood phylogenetic tree showing evolutionary relatedness of BdpA orthologs to the BAR domain prediction sequences (Supplemental Fig. 5). The 5 BdpA orthologs predicted to contain a BAR domain based on the current model were subsequently aligned with representative known BAR proteins from the various BAR domain subtypes (N-BAR, F-BAR, and I-BAR)[66]. BdpA and its prokaryotic orthologs cluster separately from the eukaryotic BAR proteins in their own distinct clade (Fig. 5), suggesting that while BdpA contains a functional BAR domain, it represents its own class of BAR domain, hereafter named P-BAR (Prokaryotic BAR). It seems likely that the P-BAR domain arose as a result of horizontal gene transfer from a eukaryote due to the prevalence of eukaryotic coiled-coil proteins with predicted homology to BdpA after 2 iterations of PSI-BLAST. However, the branch lengths and low bootstrap values supporting the placement of P-BAR relative to other BAR domain subtypes make it challenging to directly infer the evolutionary history of P-BAR domains. Discovery of other putative P-BAR proteins would help to build this analysis, and if future comparative proteomics analysis of OME/Vs demonstrates overlapping activity of BdpA with preferential cargo loading into OME/Vs, it could hint at the evolutionary origins of vesicle-based protein trafficking. Conservation of BAR domain proteins supports the notion that three-dimensional organization of proteins in lipid structures is as important to

prokaryotes as it is eukaryotes, and suggests additional novel P-BAR proteins are waiting to be discovered.

Methods

Bacterial strains, plasmids, and medium The bacterial strains used in this study can be found in Supplemental Table 1. *S. oneidensis* strains were grown aerobically in Luria Bertani (LB) media at 30˚C with 50 µg/mL kanamycin when maintaining the plasmid. To observe membrane extensions, cells were centrifuged and resuspended in a defined media comprised of 30 mM Pipes, 60 mM sodium DL-lactate as an electron donor, 28mM NH4Cl, 1.34 mM KCl, 4.35 mM NaH2PO4, 7.5 mM NaOH, 30 mM NaCl, 1mM MgCl2, 1 mM CaCl2, and 0.05 mM ferric nitrilotriacetic acid[30]. *Marinobacter atlanticus* CP1 strains were grown in BB media (50% LB media, 50% Marine broth) at 30˚C with 100 µg/mL kanamycin to maintain the plasmids as described previously[60].

Inducible BdpA expression plasmids were constructed for use in *S. oneidensis* MR-1, *M. atlanticus* CP1, and *E. coli* BL21(DE3) using the pBBR1-mcs2 backbone described previously[60]. The Marionette sensor components (*phlF* promoter, consitutively expressed PhlF repressor, and yellow fluorescence protein (YFP)) cassette from pAJM.452[57] was cloned into the pBBR1-mcs2 backbone, and the YFP cassette was replaced with the gene encoding BdpA by Gibson assembly (primers in Supplemental Table 1). The resulting plasmid was given the name p452-*bdpA*. The Gibson assembly reactions were electroporated into *E. coli* Top10 DH5α cells (Invitrogen), and the sequences were confirmed through Sanger sequencing (Eurofins genomics). Plasmid constructs were chemically transformed into conjugation-competent *E. coli* WM3064 cells

for conjugative transfer into the recipient bacterial strains of *S. oneidensis* MR-1 and *M. atlanticus* CP1. The same BdpA expression vector was transformed into *E. coli* BL21(DE3) cells (Invitrogen) by chemical transformation.

Generation of a scarless *ΔbdpA* knockout mutant of *S. oneidensis* was performed by combining 1 kilobase fragments flanking upstream and downstream from *bdpA* by Gibson assembly into the pSMV3 suicide vector. The resultant plasmid pSMV3_1507KO was transformed into *E. coli* UQ950 cells for propagation. Plasmid sequences were confirmed by Sanger sequencing before chemical transformation into *E. coli* UQ950 for conjugation into *S. oneidensis*. Conjugation of pSMV3_1507KO into *S. oneidensis* MR-1 was performed as described previously[31].

Purification of Outer Membrane Vesicles *S. oneidensis* MR-1 cells were grown in LB in 1L non-baffled flasks at 30° C at 200 RPM. When an OD_{600} of 3.0 was reached, cells were pelleted by centrifugation at 5000 x g for 20 min at 4°C, resulting supernatant was filtered through a 0.45 µm filter to remove remaining bacterial cells. Vesicles were obtained by centrifugation at 38,400 x g for 1 h at 4°C in an Avanti J-20XP centrifuge (Beckman Coulter, Inc). Pelleted vesicles were resuspended in 20 ml of 50 mM HEPES (pH 6.8) and filtered through 0.22 µm pore size filters. Vesicles were again pelleted as described above and finally resuspended in 50 mM HEPES, pH 6.8, except for vesicle preparations used for electrochemistry which were suspended in 100 mM MES, 100 mM KCl, pH 6.8. Extracellular DNA, flagella, and pili can all be co-purified. Protocol was adapted from[67].

Dynamic Light Scattering Distribution of vesicle diameters were measured with Wyatt Technology's Möbiuζ dynamic light scattering instrument.

Electrochemistry CHA Industries Mark 40 e-beam and thermal evaporator was used to deposit a 5 nm Ti adhesion layer and then a 100 nm Au layer onto cleaned glass coverslips (43X50 NO. 1 Thermo Scientific Gold Seal Cover Glass, Portsmouth NH, USA). Self-assembled monolayers were formed by incubated the gold coverslip in a solution of 1mM 6-mercaptohexanoic acid in 200 proof ethanol for at least 2 hours. Electrode was then rinsed several time in ethanol followed by several rinses in milliQ water. The SAMs layer was then activated by incubation in 100 mM N-(3-Dimethylaminopropyl)-N′-ethylcarbodiimide hydrochloride and 25 mM N-hydroxysuccinimide, pH 4, for 30 minutes. A sample of outer membrane vesicles was deposited on the surface of the electrode and incubated at room temperature overnight in a humid environment. Cyclic voltammetry was performed in a 50 mL 3 electrode half-cell completed with a platinum counter electrode, and a 1 M KCl Ag/AgCl reference electrode electrical controlled by a Gamry 600 potentiostat (Gamry, Warminster, PA). The whole experiment was completed in an anaerobic chamber with 95% nitrogen, 5% hydrogen atmosphere.

313 **Proteomics** Vesicle samples were prepared as described above. *S. oneidensis* outer
314 membrane (OM) was purified via the Sarkosyl method described by Brown et al.[68]. A 50
315 mL overnight culture of cells was harvested by centrifugation at 10,000 × g for 10 min.
316 The cell pellet suspended in 20 mL of 20 mM ice-cold sodium phosphate (pH 7.5) and
317 passed four times through a French Press (12000 lb/in^2). The lysate was centrifuged at
318 5,000 × g for 30 min to remove unbroken cells. The remaining supernatant was
319 centrifuged at 45,000 × g for 1 h to pellet membranes. Crude membranes were
320 suspended in 20 mL 0.5% Sarkosyl in 20 mM sodium phosphate and shaken horizontally
321 at 200 rpm for 30 min at room temperature. The crude membrane sample was centrifuged
322 at 45,000 × g for 1 h to pellet the OM. The pellet of OM was washed in ice-cold sodium
323 phosphate and recentrifuged.

324 To prepare for mass spectrometry samples were treated sequentially with urea,
325 TCEP, iodoactinamide, lysl endopeptidase, trypsin, and formic acid. Peptides were then
326 desalted by HPLC with a Microm Bioresources C8 peptide macrotrap (3x8mm). The
327 digested samples were subjected to LC-MS/MS analysis on a nanoflow LC system,
328 EASY-nLC 1200, (Thermo Fisher Scientific) coupled to a QExactive HF Orbitrap mass
329 spectrometer (Thermo Fisher Scientific, Bremen, Germany) equipped with a Nanospray
330 Flex ion source. Samples were directly loaded onto a PicoFrit column (New Objective,
331 Woburn, MA) packed in house with ReproSil-Pur C18AQ 1.9 um resin (120A° pore size,
332 Dr. Maisch, Ammerbuch, Germany). The 20 cm x 50 µm ID column was heated to 60°
333 C. The peptides were separated with a 120 min gradient at a flow rate of 220 nL/min.
334 The gradient was as follows: 2–6% Solvent B (7.5 min), 6-25% B (82.5 min), and 25-40%
335 B (30 min) and to 100% B (9min). Solvent A consisted of 97.8% H2O, 2% ACN, and

0.2% formic acid and solvent B consisted of 19.8% H2O, 80% ACN, and 0.2% formic acid. The QExactive HF Orbitrap was operated in data dependent mode with the Tune (version 2.7 SP1build 2659) instrument control software. Spray voltage was set to 2.5 kV, S-lens RF level at 50, and heated capillary at 275 °C. Full scan resolution was set to 60,000 at m/z 200. Full scan target was 3 × 106 with a maximum injection time of 15 ms. Mass range was set to 300−1650 m/z. For data dependent MS2 scans the loop count was 12, target value was set at 1 × 105, and intensity threshold was kept at 1 × 105. Isolation width was set at 1.2 m/z and a fixed first mass of 100 was used. Normalized collision energy was set at 28. Peptide match was set to off, and isotope exclusion was on. Data acquisition was controlled by Xcalibur (4.0.27.13) and all data was acquired in profile mode.

Bioinformatics Putative BAR domain SO_1507 (BdpA) was identified in search of annotation terms of *S. oneidensis* MR-1. The conserved domain database (CDD-search)(NCBI) was accessed to identify the position-specific scoring matrix (PSSM) that matched and specific region of SO_1507 that represented the BAR domain. It was confirmed that a region 276-421 matched to BAR superfamily cl12013 and specifically to the family member BAR cd07307. LOGICOIL multi-state coiled-coil oligomeric state prediction was used to determine the presence of coiled-coils within BdpA. SignalP 6.1 was used to detect the presence of the signal peptide and cellular localization of BdpA.

A PSI-BLAST[69] search against the NCBI nr database was performed using the BdpA BAR sequence as the initial search seed to determine how prevalent the BdpA BAR domain is in related species. Conserved BdpA orthologs were annotated as hypothetical proteins in all of the species identified. In the initial round, 24 proteins were found from

other organisms identified as *Shewanella* with a high conservation among the proteins and another 28 proteins were found in more distant bacteria species that had similarity of 65% to 44 %. A second iteration identified a few proteins much more distantly related from bacterial species and then proteins from eukaryote phylum *Arthropoda* that were annotated as being centrosomal proteins. All of the found proteins from bacterial species were hypothetical proteins with no known function. Only five of the proteins from the search returned hits to the PSSM of the BAR cd07307. The identity among the proteins was very high and examination of the proteins suggests that a functional form similar to the BAR domain would result for all the found proteins. Overall this places the original protein SO_1507 as a protein that just barely meets criteria via PSSM models to be assigned a matching the BAR domain while the rest of the proteins found have enough differences to fail to match the BAR model while still being very similar to SO_1507. An attempt was made to build up a HMM (Hidden Markov Model) using HMMer to use for searching for other proteins that might match but as with the PSI-BLAST search only the proteins that formed the model returned as good matches. So there appear to be a tight clade of very similar proteins with very little differentiation in the sequence. This indicates that while sequence homology between BdpA and the existing BAR domain consensus sequence predicted the BAR domain region in BdpA using hmmer or NCBI tools, the sequence conservation is at the cusp of a positive hit by the HMM since other closely related (>90% homology) BdpA orthologs were not predicted to contain a BAR domain by this method. The most homologous eukaryotic protein to BdpA (27%) is a putative centrosomal protein in *Vollenhovia emeryi* (accession #: XP_011868153) that is predicted to contain an amino terminal C2 membrane binding domain and a carboxy-terminal SMC

382 domain within a coiled-coil region. Despite CDD search failing to predict the presence of
383 a BAR domain in this protein, it does not preclude the presence of one, pending an
384 updated BAR pfam HMM.

385

386 **Confocal microscopy** For *in vivo* imaging of intrinsic outer membrane extension
387 production, *S. oneidensis* MR-1 strains were grown in LB media overnight, washed twice
388 with SDM, and diluted to an OD_{600} of 0.05 in 1 mL of SDM with appropriate antibiotics.
389 Prior to pipetting, ~1cm of the pipette tip was trimmed to minimize shear forces during
390 transfer. 100 µL of each culture was labeled with 1 µL 1M FM 4-64 to visualize the cell
391 membranes. After staining, 10 µL of the labeled cell suspension was gently pipetted onto
392 22 x 22 mm No.1 cover glass (VWR) and sealed onto glass slides with clear acrylic nail
393 polish (for confocal imaging) or onto chambered cover glass (for widefield fluorescence).
394 On average, intrinsic membrane extension formation could be observed starting after 45
395 minutes sealed onto cover glass. Diluted cells were induced with 12.5 µM DAPG for 1
396 hour at 30˚C with 200 RPM shaking agitation for planktonic OME production. Cells were
397 labeled with FM 4-64 and sealed onto glass slides as before. Induced OMEs were imaged
398 immediately after mounting onto slides.

399 Confocal images were taken by a Zeiss LSM 800 confocal microscope with a Plan-
400 Apochromat 63x/1.4 numerical aperture oil immersion M27 objective. FM 4-64
401 fluorescence was excited at 506 nm: 0.20% laser power. Emission spectra was detected
402 from 592-700 nm using the LSM 800 GaAsP-Pmt2 detector. To capture the dynamics of
403 the OMEs, images were collected over the designated length of time between 0.27 – 0.63
404 seconds per frame. Single frame time series images were collected of either a 50.71 µm

by 50.71 µm (2x zoom) or a 20.28 µm by 20.28 µm (5x zoom) field of view. Images were recorded using the Zeiss Zen software (Carl Zeiss Microscopy, LLC, Thornwood, NY, USA).

Perfusion flow microscopy For OME statistics comparing *S. oneidensis* strains MR-1 and Δ*bdpA,* cells were pre-grown aerobically from frozen (-80°C) stock in 10 mL of Luria-Bertani (LB) broth (supplemented with 50 µg/mL Kanamycin for strains with plasmid) in a 125-mL flask overnight at 30°C and 225 rpm. The next day, the stationary phase (OD_{600} 3.0 – 3.3) preculture was used to inoculate 1:100 into 10 mL of fresh LB medium in a 125-mL flask. After ~6 hours at 30°C and 225 rpm, when the OD_{600} was 2.4 (late log phase), 5 mL of cells were collected by centrifugation at 4226 x *g* for 5 min and washed twice in defined medium. The perfusion chamber, microscope, and flow medium described previously[7,29,30] were used for all perfusion flow OME statistics experiments. During each 5 hour imaging experiment, the perfusion chamber was first filled with this flow medium, then <1 mL of washed cells were slowly injected for a surface density of ~100-300 cells per 112 x 112 µm field of view on a Nikon Ti-E inverted microscope. Cells were allowed to attach for 5-15 minutes on the coverslip before perfusion flow was resumed at a volumetric flow rate of 6.25 ± 0.1 µL/s. Cells and OMEs were visualized with the red membrane stain FM 4-64FX in the flow medium (0.25 µg/mL of flow medium). A total of 1,831 wild type and 2,265 Δ*bdpA* cells were used for extension and vesicle quantification.

Cryo transmission electron microscopy

Shewanella strains were streaked onto LB plates with or without kanamycin and allowed to incubate 3 days on a benchtop. The night before freezing, individual colonies were

inoculated into 3 ml LB +/- kanamycin and incubated at 30 °C overnight with 200 rpm shaking. The following morning optical densities of the cultures were measured at 600nm and adjusted to a final OD_{600} of 1. Cells were pelleted at 8,000 rpm for three minutes for buffer exchange/washes. For the Δ*bdpA*_p452-*bdpA* transformed cells, 12.5 µM DAPG was added. A freshly glow discharged 200 mesh copper grid with R2/1 Quantifoil carbon film was placed into a concavity slide. Approximately 150 µl of a 1:10 dilution of the cell suspensions, with or without the inducer, was added to cover the grid. A glass coverslip was then lowered onto the concavity to exclude air bubbles. The edges of the coverslip were then sealed with nail polish to prevent media evaporation. The slide assembly was then incubated in a 30 °C incubator for 1.5 to 3 hours. Immediately prior to plunge freezing, the top coverslip was removed by scoring the nail polish with a razor blade. TEM grids with cells were gently retrieved with forceps and loaded into a Leica grid plunge for automated blotting and plunging into LN_2-cooled liquid ethane. Vitrified grids were transferred to a LN_2 storage dewar. Imaging of frozen samples was performed on either a Titan (ThermoFisher Scientific) microscope equipped with a Gatan Ultrascan camera and operating at 300 kV or a Talos (ThermoFisher Scientific) equipped with a Ceta camera and operating at 200 kV. Images were acquired at 10,000 to 20,000 X magnification and were adjusted by bandpass filtering.

Acknowledgements

We thank Dr. Jeffery Gralnick for helpful discussions and advice; Dr. Adam Meyer and Dr. Chris Voigt for the DAPG-inducible Marionette promoter; Dr. Annie Moradian and

Dr. Mike Sweredoski and the California Institute of Technology Proteome Exploration Lab for useful discussions on the preparation and analysis of proteomics data. Some of the cryo-TEM work was done in the Beckman Institute Resource Center for Transmission Electron Microscopy at Caltech. This work was supported by the United States Department of Defense Synthetic Biology for Military Environments (SBME) Applied Research for the Advancement of Science and Technology Priorities (ARAP) program. Work in ME-N's lab was supported by the U.S. Office of Naval Research Multidisciplinary University Research Initiative Grant No. N00014-18-1-2632. LAZ was partially supported by the National Science Foundation grant DEB-1542527. SX was supported by the Division of Chemical Sciences, Geosciences, and Biosciences, Office of Basic Energy Sciences of the U.S. Department of Energy through grant DE-FG02-13ER16415. Work in GJJ's lab was supported by the National Institute of Health (GM122588 to GJJ).

Author Contributions

DP and LZ conceived the study independently then combined projects when complementary data on BdpA was discovered. LZ purified OMVs, prepared samples for LC MS-MS, and performed DLS measurements. LZ and SX made electrochemical measurements and analysis. DP conducted BdpA domain prediction and validation analysis, generated the p452-*bdpA* plasmid, Δ*bdpA* and p452-*bdpA* strains. DP and GC conducted fluorescence and confocal imaging experiments, and DP, LZ, and GC analyzed the data. LB adapted the Marionette sensor (P_{phlF}-YFP) into pBBR1-mcs2. LZ and LAM performed cryo-TEM of OMVs. GC conducted perfusion flow imaging experiments. GC and LZ analyzed perfusion flow system data. CH, DP, and LD performed cryo-TEM experiments of OMEs and image processing / analysis. DP and AM

474 generated phylogenetic data, and DP, AM, and BE analyzed the data. DP, LZ, CM, GC,
475 AM, LAM, BE, GJJ, LD, MEN, and SG provided data interpretation. DP, LZ, MEN, and
476 SG wrote the manuscript, with input from all coauthors.

References

1 Carman, P. J. & Dominguez, R. BAR domain proteins-a linkage between cellular membranes, signaling pathways, and the actin cytoskeleton. *Biophys Rev* **10**, 1587-1604, (2018).

2 Schoneberg, J. *et al.* Lipid-mediated PX-BAR domain recruitment couples local membrane constriction to endocytic vesicle fission. *Nat Commun* **8**, 15873, (2017).

3 van Weering, J. R. & Cullen, P. J. Membrane-associated cargo recycling by tubule-based endosomal sorting. *Semin Cell Dev Biol* **31**, 40-47, (2014).

4 Knaevelsrud, H. *et al.* Membrane remodeling by the PX-BAR protein SNX18 promotes autophagosome formation. *J Cell Biol* **202**, 331-349, (2013).

5 Mim, C. & Unger, V. M. Membrane curvature and its generation by BAR proteins. *Trends Biochem Sci* **37**, 526-533, (2012).

6 Rao, Y. & Haucke, V. Membrane shaping by the Bin/amphiphysin/Rvs (BAR) domain protein superfamily. *Cell Mol Life Sci* **68**, 3983-3993, (2011).

7 Chong, G. W., Pirbadian, S. & El-Naggar, M. Y. Surface-Induced Formation and Redox-Dependent Staining of Outer Membrane Extensions in Shewanella oneidensis MR-1. *Frontiers in Energy Research* **7**, (2019).

8 Fischer, T. *et al.* Biopearling of Interconnected Outer Membrane Vesicle Chains by a Marine Flavobacterium. *Appl Environ Microbiol* **85**, (2019).

9 Toyofuku, M., Nomura, N. & Eberl, L. Types and origins of bacterial membrane vesicles. *Nature Reviews Microbiology*, (2018).

10 Hampton, C. M. *et al.* The Opportunistic Pathogen Vibrio vulnificus Produces Outer Membrane Vesicles in a Spatially Distinct Manner Related to Capsular Polysaccharide. *Front Microbiol* **8**, 2177, (2017).

11 Kim, E. Y., Tyndall, E. R., Huang, K. C., Tian, F. & Ramamurthi, K. S. Dash-and-Recruit Mechanism Drives Membrane Curvature Recognition by the Small Bacterial Protein SpoVM. *Cell Syst* **5**, 518-526 e513, (2017).

12 Cornejo, E., Subramanian, P., Li, Z., Jensen, G. J. & Komeili, A. Dynamic Remodeling of the Magnetosome Membrane Is Triggered by the Initiation of Biomineralization. *MBio* **7**, e01898-01815, (2016).

13 Bohuszewicz, O., Liu, J. & Low, H. H. Membrane remodelling in bacteria. *J Struct Biol* **196**, 3-14, (2016).

14 Remis, J. P. *et al.* Bacterial social networks: structure and composition of Myxococcus xanthus outer membrane vesicle chains. *Environ Microbiol* **16**, 598-610, (2014).

15 Wei, X., Vassallo, C. N., Pathak, D. T. & Wall, D. Myxobacteria produce outer membrane-enclosed tubes in unstructured environments. *J Bacteriol* **196**, 1807-1814, (2014).

16 Low, H. H., Sachse, C., Amos, L. A. & Lowe, J. Structure of a bacterial dynamin-like protein lipid tube provides a mechanism for assembly and membrane curving. *Cell* **139**, 1342-1352, (2009).

17 Peter, B. J. *et al.* BAR domains as sensors of membrane curvature: the amphiphysin BAR structure. *Science* **303**, 495-499, (2004).

18 Frost, A., De Camilli, P. & Unger, V. M. F-BAR proteins join the BAR family fold. *Structure* **15**, 751-753, (2007).

19 Shimada, A. *et al.* Curved EFC/F-BAR-domain dimers are joined end to end into a filament for membrane invagination in endocytosis. *Cell* **129**, 761-772, (2007).

20 Weissenhorn, W. Crystal structure of the endophilin-A1 BAR domain. *J Mol Biol* **351**, 653-661, (2005).
21 Drin, G. & Antonny, B. Amphipathic helices and membrane curvature. *FEBS Lett* **584**, 1840-1847, (2010).
22 Seet, L. F. & Hong, W. The Phox (PX) domain proteins and membrane traffic. *Biochim Biophys Acta* **1761**, 878-896, (2006).
23 Itoh, T. & De Camilli, P. BAR, F-BAR (EFC) and ENTH/ANTH domains in the regulation of membrane-cytosol interfaces and membrane curvature. *Biochim Biophys Acta* **1761**, 897-912, (2006).
24 Simunovic, M., Voth, G. A., Callan-Jones, A. & Bassereau, P. When Physics Takes Over: BAR Proteins and Membrane Curvature. *Trends Cell Biol* **25**, 780-792, (2015).
25 Mim, C. *et al.* Structural basis of membrane bending by the N-BAR protein endophilin. *Cell* **149**, 137-145, (2012).
26 Habermann, B. The BAR-domain family of proteins: a case of bending and binding? *EMBO reports* **5**, 250-255, (2004).
27 Miki, H., Yamaguchi, H., Suetsugu, S. & Takenawa, T. IRSp53 is an essential intermediate between Rac and WAVE in the regulation of membrane ruffling. *Nature* **408**, 732-735, (2000).
28 Sampath, V., McCaig, W. D. & Thanassi, D. G. Amino acid deprivation and central carbon metabolism regulate the production of outer membrane vesicles and tubes by Francisella. *Mol Microbiol* **107**, 523-541, (2018).
29 Subramanian, P., Pirbadian, S., El-Naggar, M. Y. & Jensen, G. J. Ultrastructure of Shewanella oneidensis MR-1 nanowires revealed by electron cryotomography. *Proc Natl Acad Sci U S A* **115**, E3246-E3255, (2018).
30 Pirbadian, S. *et al.* Shewanella oneidensis MR-1 nanowires are outer membrane and periplasmic extensions of the extracellular electron transport components. *Proc Natl Acad Sci U S A* **111**, 12883-12888, (2014).
31 Gorby, Y. A. *et al.* Electrically conductive bacterial nanowires produced by Shewanella oneidensis strain MR-1 and other microorganisms. *Proc Natl Acad Sci U S A* **103**, 11358-11363, (2006).
32 Bhattacharya, S. *et al.* A Ubiquitous Platform for Bacterial Nanotube Biogenesis. *Cell Rep*, (2019).
33 Dubey, G. P. *et al.* Architecture and Characteristics of Bacterial Nanotubes. *Dev Cell* **36**, 453-461, (2016).
34 Dubey, G. P. & Ben-Yehuda, S. Intercellular nanotubes mediate bacterial communication. *Cell* **144**, 590-600, (2011).
35 Pande, S. *et al.* Metabolic cross-feeding via intercellular nanotubes among bacteria. *Nat Commun* **6**, 6238, (2015).
36 Tanaka, M., Arakaki, A. & Matsunaga, T. Identification and functional characterization of liposome tubulation protein from magnetotactic bacteria. *Mol Microbiol* **76**, 480-488, (2010).
37 Danne, L. *et al.* Membrane Remodeling by a Bacterial Phospholipid-Methylating Enzyme. *MBio* **8**, (2017).
38 Danne, L. *et al.* Dissection of membrane-binding and -remodeling regions in two classes of bacterial phospholipid N-methyltransferases. *Biochim Biophys Acta* **1859**, 2279-2288, (2017).
39 Danne, L. *et al.* Membrane-binding mechanism of a bacterial phospholipid N-methyltransferase. *Mol Microbiol* **95**, 313-331, (2015).
40 Low, H. H. & Lowe, J. A bacterial dynamin-like protein. *Nature* **444**, 766-769, (2006).
41 Nealson, K. H. & Scott, J. Ecophysiology of the Genus Shewanella. 1133-1151, (2006).
42 Marsili, E. *et al.* Shewanella secretes flavins that mediate extracellular electron transfer. *Proceedings of the National Academy of Sciences* **105**, 3968-3973, (2008).

43 Gorby, Y. *et al.* Redox-reactive membrane vesicles produced by Shewanella. *Geobiology* **6**, 232-241, (2008).

44 Liu, X. *et al.* Bacterial Vesicles Mediate Extracellular Electron Transfer. *Environmental Science & Technology Letters*, (2019).

45 Xu, S., Barrozo, A., Tender, L. M., Krylov, A. I. & El-Naggar, M. Y. Multiheme Cytochrome Mediated Redox Conduction through Shewanella oneidensis MR-1 Cells. *J Am Chem Soc* **140**, 10085-10089, (2018).

46 Okamoto, A., Nakamura, R. & Hashimoto, K. In-vivo identification of direct electron transfer from Shewanella oneidensis MR-1 to electrodes via outer-membrane OmcA–MtrCAB protein complexes. *Electrochimica Acta* **56**, 5526-5531, (2011).

47 Cox, J. *et al.* Accurate proteome-wide label-free quantification by delayed normalization and maximal peptide ratio extraction, termed MaxLFQ. *Mol Cell Proteomics* **13**, 2513-2526, (2014).

48 Hsu, V. W., Bai, M. & Li, J. Getting active: protein sorting in endocytic recycling. *Nat Rev Mol Cell Biol* **13**, 323-328, (2012).

49 Vincent, T. L., Green, P. J. & Woolfson, D. N. LOGICOIL--multi-state prediction of coiled-coil oligomeric state. *Bioinformatics* **29**, 69-76, (2013).

50 Linkner, J. *et al.* The inverse BAR domain protein IBARa drives membrane remodeling to control osmoregulation, phagocytosis and cytokinesis. *J Cell Sci* **127**, 1279-1292, (2014).

51 Cui, H. *et al.* Understanding the role of amphipathic helices in N-BAR domain driven membrane remodeling. *Biophys J* **104**, 404-411, (2013).

52 Henne, W. M. *et al.* Structure and analysis of FCHo2 F-BAR domain: a dimerizing and membrane recruitment module that effects membrane curvature. *Structure* **15**, 839-852, (2007).

53 Pylypenko, O., Lundmark, R., Rasmuson, E., Carlsson, S. R. & Rak, A. The PX-BAR membrane-remodeling unit of sorting nexin 9. *EMBO J* **26**, 4788-4800, (2007).

54 Vinogradov, E., Korenevsky, A. & Beveridge, T. J. The structure of the rough-type lipopolysaccharide from Shewanella oneidensis MR-1, containing 8-amino-8-deoxy-Kdo and an open-chain form of 2-acetamido-2-deoxy-d-galactose. *Carbohydrate Research* **338**, 1991-1997, (2003).

55 Toyofuku, M., Tashiro, Y., Hasegawa, Y., Kurosawa, M. & Nomura, N. Bacterial membrane vesicles, an overlooked environmental colloid: Biology, environmental perspectives and applications. *Adv Colloid Interface Sci* **226**, 65-77, (2015).

56 Tran, F. & Boedicker, J. Q. Genetic cargo and bacterial species set the rate of vesicle-mediated horizontal gene transfer. *Sci Rep* **7**, 8813, (2017).

57 Meyer, A. J., Segall-Shapiro, T. H., Glassey, E., Zhang, J. & Voigt, C. A. Escherichia coli "Marionette" strains with 12 highly optimized small-molecule sensors. *Nat Chem Biol*, (2018).

58 Mahmood, M. I., Noguchi, H. & Okazaki, K. I. Curvature induction and sensing of the F-BAR protein Pacsin1 on lipid membranes via molecular dynamics simulations. *Sci Rep* **9**, 14557, (2019).

59 Wang, Q. *et al.* Molecular mechanism of membrane constriction and tubulation mediated by the F-BAR protein Pacsin/Syndapin. *Proc Natl Acad Sci U S A* **106**, 12700-12705, (2009).

60 Bird, L. J. *et al.* Development of a Genetic System for Marinobacter atlanticus CP1 (sp. nov.), a Wax Ester Producing Strain Isolated From an Autotrophic Biocathode. *Front Microbiol* **9**, 3176, (2018).

61 Coursolle, D. & Gralnick, J. A. Modularity of the Mtr respiratory pathway of Shewanella oneidensis strain MR-1. *Mol Microbiol* **77**, 995-1008, (2010).

62 Bird, L. J. *et al.* Engineered living conductive biofilms as functional materials. *MRS Communications*, 1-13, (2019).

63 Ayton, G. S. *et al.* New insights into BAR domain-induced membrane remodeling. *Biophys J* **97**, 1616-1625, (2009).

64 Simunovic, M. *et al.* Protein-mediated transformation of lipid vesicles into tubular networks. *Biophys J* **105**, 711-719, (2013).

65 Noguchi, H. Membrane tubule formation by banana-shaped proteins with or without transient network structure. *Sci Rep* **6**, 20935, (2016).

66 Salzer, U., Kostan, J. & Djinovic-Carugo, K. Deciphering the BAR code of membrane modulators. *Cell Mol Life Sci* **74**, 2413-2438, (2017).

67 Perez-Cruz, C. *et al.* New type of outer membrane vesicle produced by the Gram-negative bacterium Shewanella vesiculosa M7T: implications for DNA content. *Appl Environ Microbiol* **79**, 1874-1881, (2013).

68 Brown, R. N., Romine, M. F., Schepmoes, A. A., Smith, R. D. & Lipton, M. S. Mapping the subcellular proteome of Shewanella oneidensis MR-1 using sarkosyl-based fractionation and LC-MS/MS protein identification. *J Proteome Res* **9**, 4454-4463, (2010).

69 Altschul, S. F. *et al.* Gapped BLAST and PSI-BLAST: a new generation of protein database search programs. *Nucleic Acids Res* **25**, 3389-3402, (1997).

636

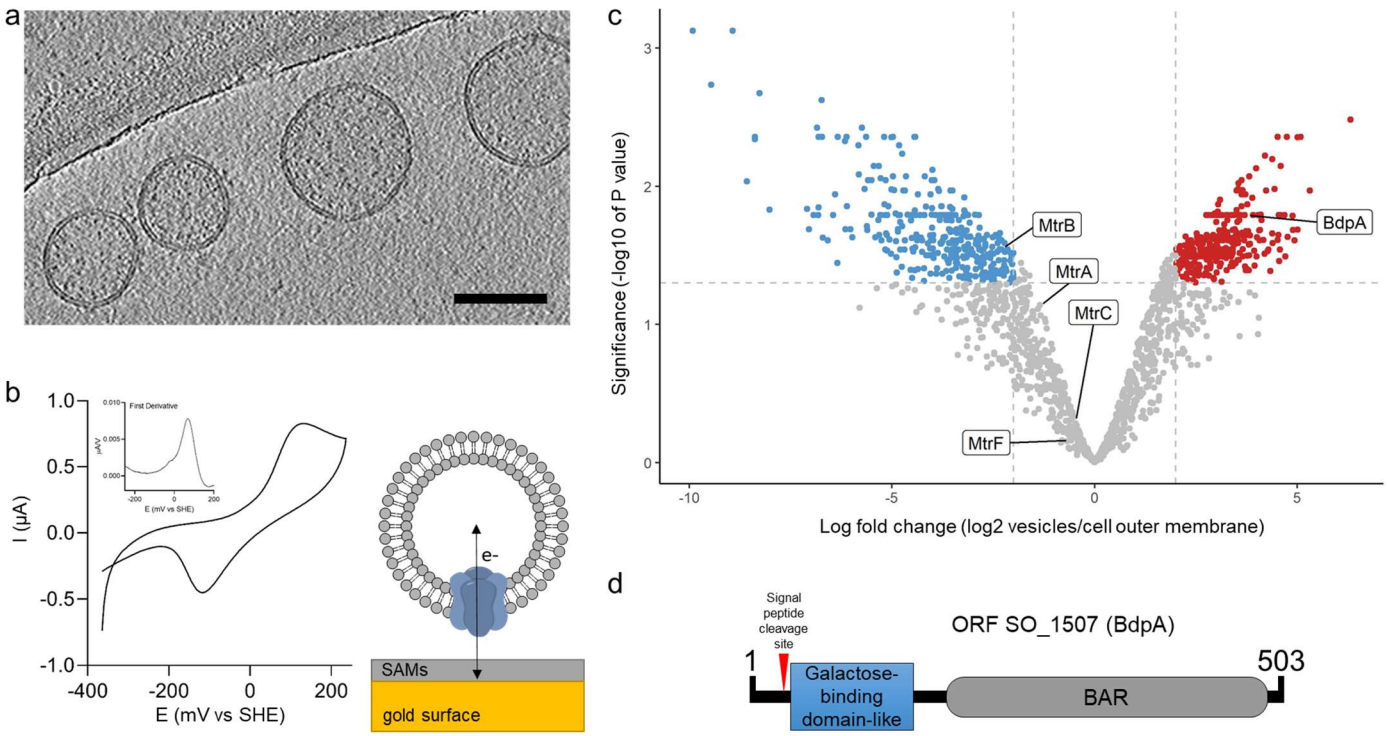

637

638 **Figure 1** Redox active vesicles are enriched with BAR domain protein BdpA. A. Cryo-TEM
639 of *S. oneidensis* MR-1 extra cellular vesicles (scale = 200 nm). B. Cyclic voltammetry of
640 vesicles adhered to gold electrode via small self-assembled monolayers, as diagramed.
641 Inset shows first derivative of anodic scan. C. Volcano plot of vesicle proteome compared
642 to cell-associated outer membrane. D. Schematic of BbdA domains.

643

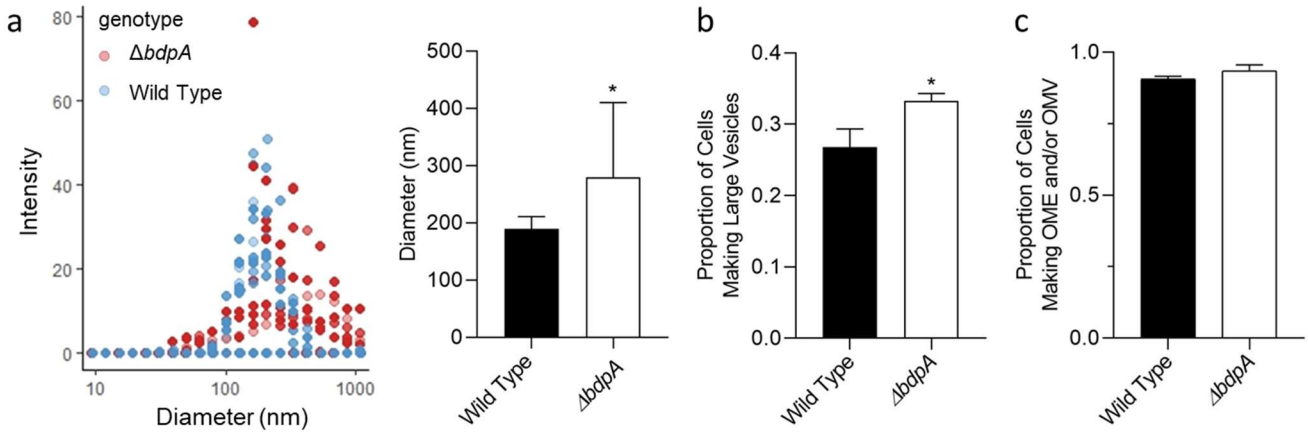

644

645 **Figure 2** BdpA is responsible for maintaining vesicle morphology but does not alter the
646 frequency of OMV or OME formation. A. Dynamic light scattering of deletion strain
647 compared to wild type, with weighted averages of vesicle size (p = 0.038). B.
648 Quantification of large vesicles being produced by living cells monitored by fluorescence
649 microscopy. C. Quantification of total number of vesicles and extensions being formed by
650 living cells as observed my fluorescence microscopy. Error bars represent standard
651 deviation.

652

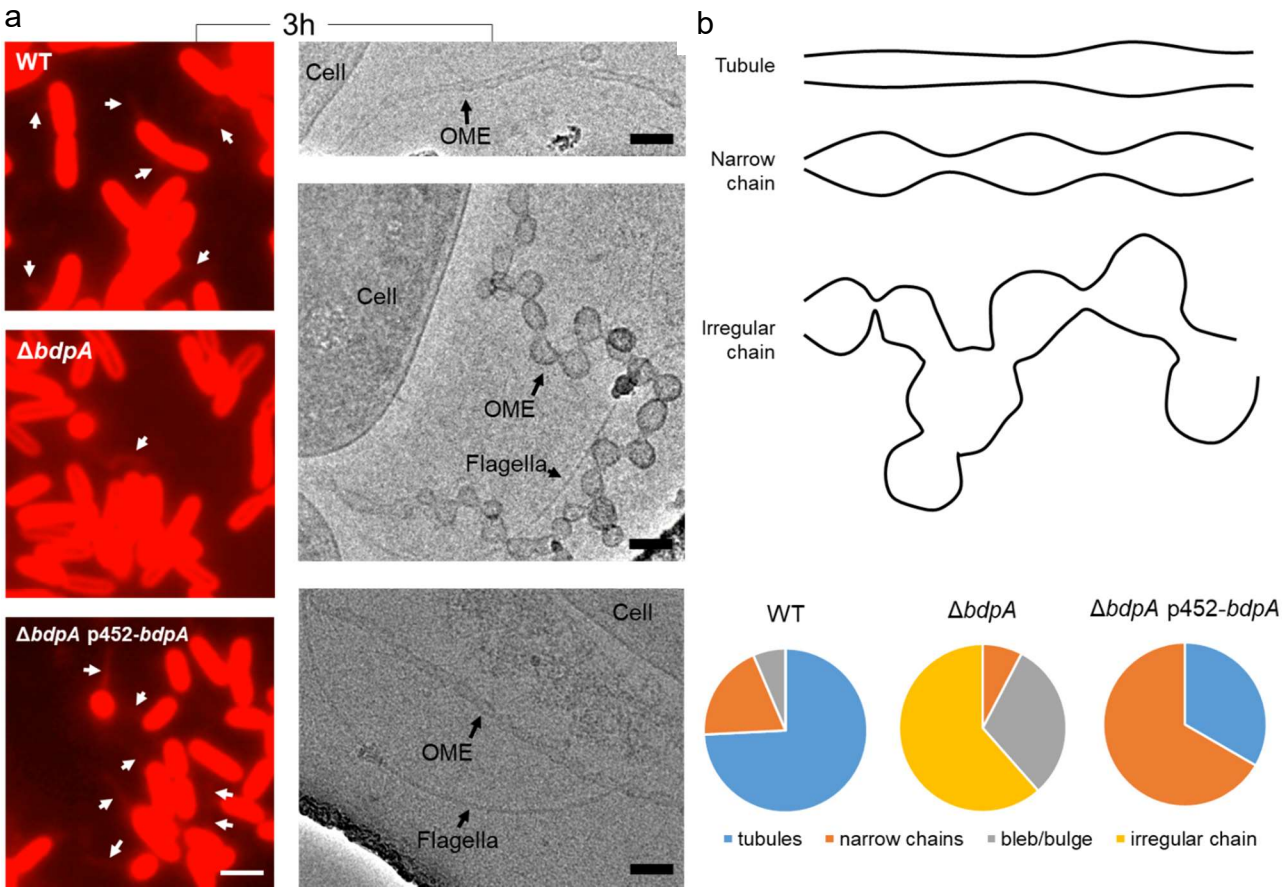

Figure 3 BdpA promotes OME maturation into ordered tubules. A) Fluorescence microscopy (left) and cryo-TEM (right) images of *S. oneidensis* WT (top), Δ*bdpA* (middle), and Δ*bdpA* p452-*bdpA* (bottom) OMEs. Scale = 2 μm (left), 100 nm (right). B) Representative cartoon of OME phenotypes and relative phenotype frequency per outer membrane structure observed from each strain. Membrane blebs/bulges were defined as non-structured membrane protrusions that did not resemble either of the other OME categories.

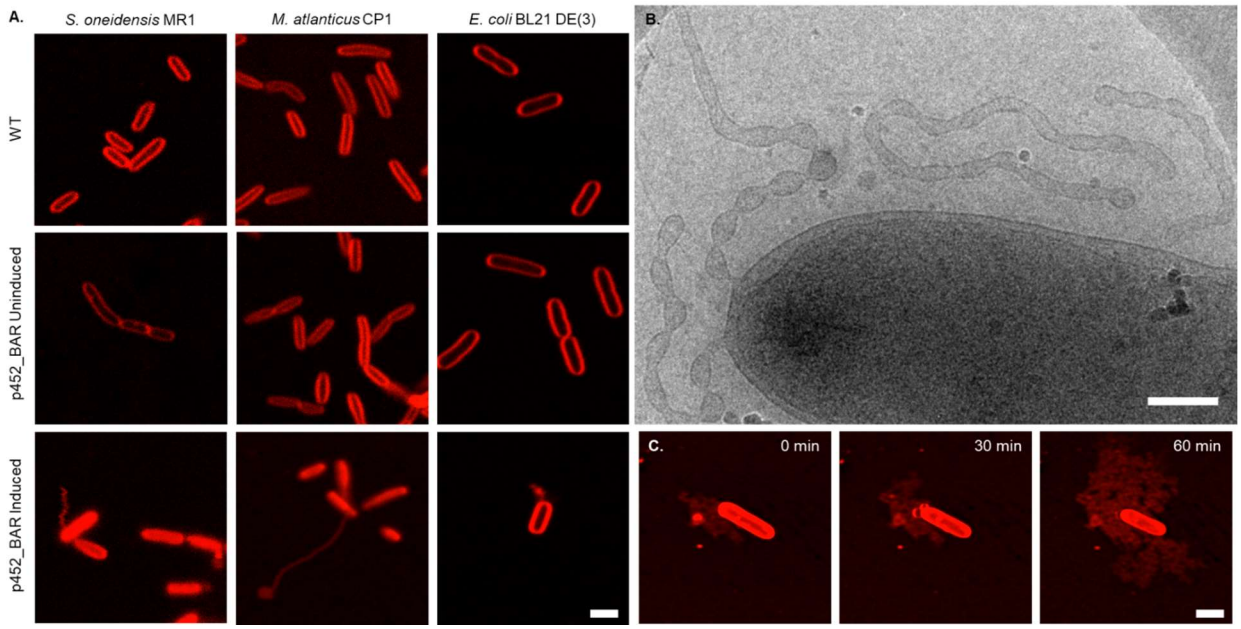

Figure 4 Heterologous expression of BdpA promotes OME formation. A) Induction of BdpA expression during planktonic, non-attached growth results in OME formation in *S. oneidensis* (left), *M. atlanticus* CP1 (middle), and *E. coli* BL21 DE(3) (right). Scale = 2 μm. B) Cryo-TEM image of planktonic *S. oneidensis* OMEs upon induction of BdpA. Scale = 200 nm. C) OME growth over time at 30 minute intervals of *E. coli* BL21 DE(3) expressing BdpA while attached to a glass surface. Scale = 2 μm.

670

671

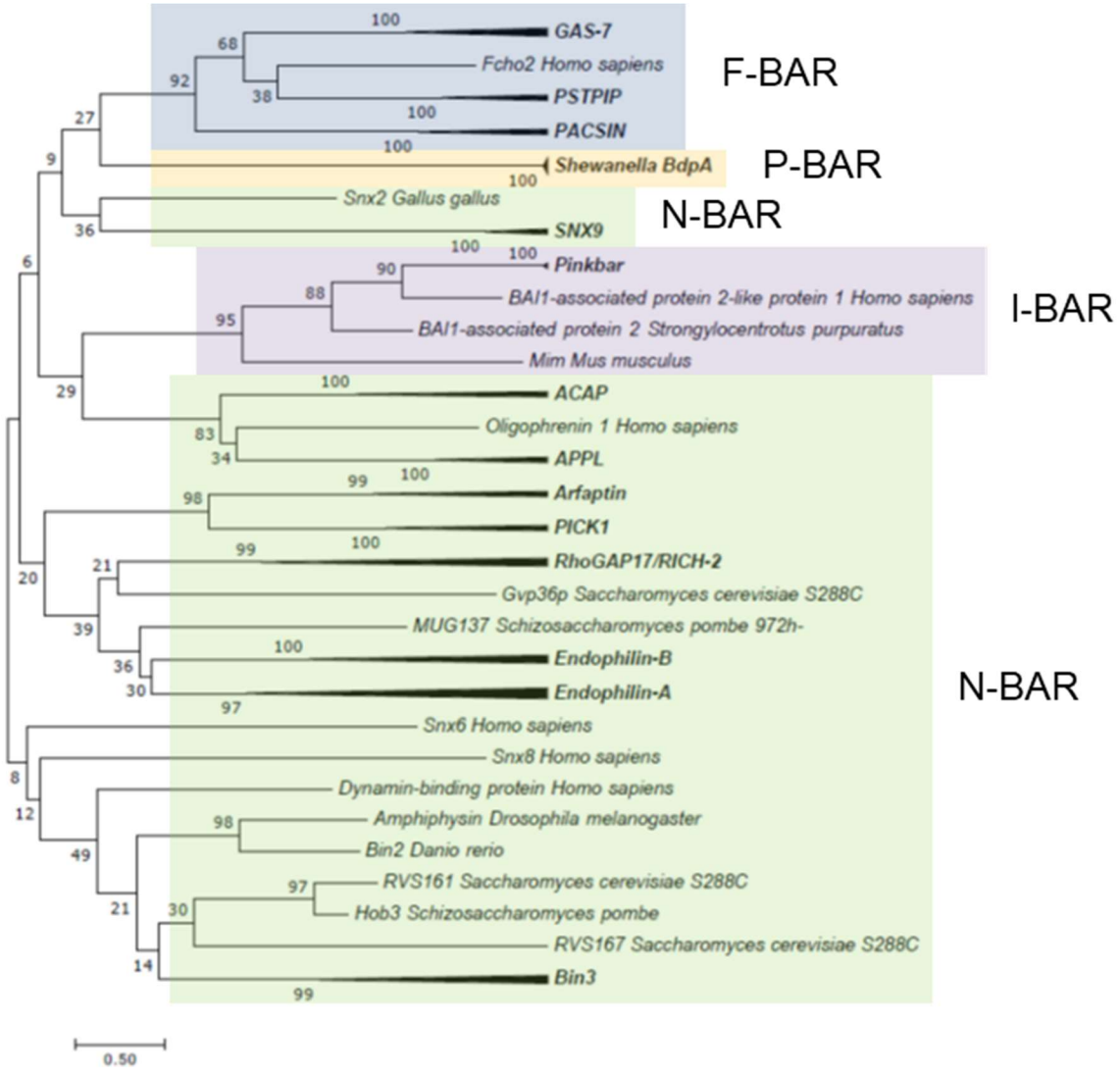

672 **Figure 5** Comparative phylogenetic analysis of BdpA with prokaryotic orthologs and eukaryotic
673 BAR domains. Maximum Likelihood evolutionary histories were inferred from 1000 bootstrap
674 replicates, and the percentage of trees in which the taxa clustered together is shown next to the
675 branches. Arrows indicate multiple branches collapsed to a single node, where arrow height is
676 relative to the number of taxa enclosed within the arrow. *S. oneidensis* BdpA and 5 prokaryotic
677 orthologs (WP_011623497 – unclassified *Shewanella* genus, ESE40074 – *S. decolorationis* S12,
678 WP_039978560 - *S. decolorationis*, KEK29176 – *S. xiamenensis*, and WP_055648003 –
679 *Shewanella sp.* Sh95) predicted by the current BAR domain pfam HMM to contain a BAR domain
680 aligned with representative BAR domains from various BAR domain subtypes (N-BAR, F-BAR, I-
681 BAR).